

Frequency-based brain networks: From a multiplex framework to a full multilayer description

J. M. Buldú^{1,2} and Mason A. Porter^{3,4,5}

¹Laboratory of Biological Networks, Center for Biomedical Technology (UPM), 28223, Pozuelo de Alarcón, Madrid, Spain

²Complex Systems Group & G.I.S.C., Universidad Rey Juan Carlos, 28933 Móstoles, Madrid, Spain

³Department of Mathematics, University of California Los Angeles, Los Angeles, USA

⁴Oxford Centre for Industrial and Applied Mathematics,

Mathematical Institute, University of Oxford, Oxford OX2 6GG, UK

⁵CABDyN Complexity Centre, University of Oxford, Oxford OX1 1HP, UK

We explore how to study dynamical interactions between brain regions using functional multilayer networks whose layers represent the different frequency bands at which a brain operates. Specifically, we investigate the consequences of considering the brain as a multilayer network in which all brain regions can interact with each other at different frequency bands, instead of as a multiplex network, in which interactions between different frequency bands are only allowed within each brain region and not between them. We study the second smallest eigenvalue of the combinatorial supra-Laplacian matrix of the multilayer network in detail, and we thereby show that the heterogeneity of interlayer edges and, especially, the fraction of missing edges crucially modify the spectral properties of the multilayer network. We illustrate our results with both synthetic network models and real data sets obtained from resting state magnetoencephalography. Our work demonstrates an important issue in the construction of frequency-based multilayer brain networks.

PACS numbers: 89.75.Hc,87.19.La,87.18.Sn

INTRODUCTION

During the last few years, network science has undergone a conceptual revolution thanks to the extension of well-established techniques of network analysis to multilayer networks [1–3], which provide a convenient way to simultaneously model different types of interactions, subsystems, and more in networks. Consequently, it has been necessary to revisit our intuitive understanding of both different structural and dynamical properties of networks — including structural phase transitions, [4], diffusion and other spreading processes [5–7], percolation and robustness [8, 9], synchronization [10], and others — to the new possibilities in multilayer descriptions, leading in many cases to counter-intuitive results.

The study of brain networks is currently undergoing a process of adaptation of classical single-layer (“monolayer”) concepts and analyses to a more general multilayer description [11, 12]. Some studies have considered integration of data coming from structural and functional brain imaging into a multilayer network to account for both anatomical and dynamical information. In an early study using monolayer networks, [13] showed that a dynamical model simulated over the anatomical network of a macaque neocortex allows one to successfully identify the positions of the anatomical hubs when signals are averaged appropriately. More recently, Stam et al. [14] analyzed how anatomical networks support activity, leading to specific functional networks (either undirected ones or directed ones), demonstrating that a dynamical model close to a critical transition is able to unveil interactions between structural and functional networks.

It is possible to analyze the organization of just a few nodes, instead of an entire network. Battiston et al. [15]

examined network motifs (i.e., overrepresented network substructures, which traditionally are composed of a few nodes [16]) that combine the anatomical connections (in one layer) and functional relations between cortical regions (in a second layer), linking data sets obtained, respectively, from diffusion magnetic resonance imaging (DW-MRI) and functional magnetic resonance imaging (fMRI).

Efforts to join anatomical and functional networks into a single multilayer network face the challenge of how to normalize the weights of edges that arise from different origins. To tackle this issue, Simas et al. [17] proposed translating functional and anatomical networks into a common embedding space and then comparing them in that space. They constructed functional networks (each with N nodes) from the fMRIs of n healthy individuals. They then used the functional networks of the n individuals to construct a single functional multiplex network, a special type of multilayer network in which corresponding entities (brain regions) in different layers (individuals) can be connected to each other via interlayer edges but other types of interlayer edges cannot occur [1]. They followed a similar procedure to construct an anatomical multiplex network using data obtained from DW-MRI. In each case independently, the multiplex networks were then projected into a common embedding space using a series of algebraic operations that allow one to calculate a so-called “algebraic aggregation” of all layers into a single layer. (See [17] for details.) Using such a projection, it is possible to quantify the differences between anatomical and functional networks. The authors also calculated an “averaged aggregation” of the functional and anatomical multiplex networks by averaging the weights of the corresponding edges over all layers. They compared the

two types of aggregation, and they were thereby able to identify certain brain regions with significant differences between the functional and anatomical networks, no matter the type of aggregation (e.g., regions related to visual, auditory, and self-awareness processes). However, only the algebraic aggregation was able to detect differences between the functional and anatomical networks in other regions (thalamus, amygdala, the postcentral gyrus, and the posterior cingulate), suggesting that averaged aggregation disregards significant information [17].

One possible alternative for reducing the complexity of analysis is to concentrate only on “functional” (dynamical, in fact) interactions between brain regions and to define multilayer functional networks as the concatenation of a series of layers, each of which captures the interplay between brain regions during some time window. This approach, in which a layer in a multilayer network represents connection similarities over some time window, was taken in papers such as [18, 19] to analyze the temporal evolution of network modules and assess dynamic reconfiguration and “flexibility” of functional networks.

Another alternative is to construct functional multilayer networks whose layers correspond to the well-known frequency bands at which a brain operates [20]. As demonstrated by Brookes et al. [21], it is possible to construct *frequency-based multilayer networks* from magnetoencephalographic (MEG) recordings by (i) band-pass filtering the raw MEG signals, (ii) obtaining the envelope of the amplitude at each frequency band, and (iii) measuring the correlations between all envelopes (for whichever frequency they account). In this way, [21] obtained frequency-based multilayer networks, in which each layer includes the interactions in a given frequency band, and showed that the corresponding supra-adjacency matrices (which encode the linear-algebraic representation of connections in a multilayer network) convey statistically significant differences when comparing a control group with a group of schizophrenia sufferers.

Very recently, De Domenico et al. took the important step of analyzing the spectral properties of frequency-based multiplex networks [22]. They compared a group of schizophrenic patients with a control group using fMRI data, and they found that the second smallest eigenvalue (i.e., *algebraic connectivity* or Fiedler value [23]) λ_2 of the combinatorial supra-Laplacian matrix associated with the multiplex network is a better discriminator between the two groups than what one can obtain by analyzing the unfiltered or single-band functional networks (i.e., by using monolayer networks). De Domenico et al. also calculated centrality measures (i.e., measures of the importance of network components [24]) on the frequency-based multiplex networks to demonstrate the existence of hubs that had not been classified previously as important brain regions for functional integration. Hubs of the control group were located in anterior cingulate, superior frontal, insula, and superior temporal cortices, but those for to schizophrenic patients were

distributed over frontal, parietal, and occipital cortices. These results reveal that frequency-based multiplex networks include relevant information about the functional organization of brain networks that is not captured by a classical monolayer approach.

In this paper, we investigate how to translate the dynamics of different brain regions into a frequency-based (i.e., functional) multilayer network, in which individual layers account for coordination within a given frequency band. We focus in particular on the consequences of analyzing a multiplex network versus a more general multilayer one. The former allow interlayer connections only between the the same brain region in different network layers, so coupling between oscillations in different frequency bands occurs only between the same brain region, whereas the latter allows one to model coordination between any brain region at any frequency band. We use resting-state MEG recordings because of their high temporal resolution (on the order of milliseconds), which makes it possible to analyze a broad spectrum of frequency bands [25, 26]. In our case, MEG signals consist of $N \approx 250$ time series, each of which is obtained from a sensor that captures the activity above a different cortical region. We then filter signals at four frequency bands (theta, alpha, beta, and gamma) and construct a 4-layer functional multilayer network from the dynamical coordination within and between frequency bands.

Combining numerical simulations with several synthetic network models and analyzing data sets from laboratory experiments, we investigate the effects that heterogeneity of interlayer edges weights have on the spectral properties of both multiplex and more general multilayer networks. In particular, we focus on the algebraic connectivity λ_2 , which is closely related to both structural and dynamical properties of networks [23, 24]. On one hand, algebraic connectivity is an indicator of modular structure in networks [27]; in the framework of multilayer networks, one can interpret the value of λ_2 and how it changes as a function of interlayer coupling strength as a way to quantify structural integration and segregation of different network layers [4]. On the other hand, $1/\lambda_2$ is proportional to the time required to reach equilibrium in a linear diffusion process [7]. Additionally, the time t_{sync} to reach synchronization of an ensemble of phase oscillators that are linearly and diffusively coupled is also proportional to $1/\lambda_2$, and it is known that t_{sync} and $1/\lambda_2$ are positively correlated in some cases with nonlinear coupling [28]. We show how the fact that a considerable fraction of all possible interlayer edges are not present in multiplex networks leads to a deviation from the theoretical values expected for λ_2 , and we investigate how these deviations are related to the mean weight of the interlayer edges. We thereby investigate the consequences of using a multiplex formalism, in which only cross-frequency coupling inside the same brain region is allowed, instead of employing a fully multilayer approach (i.e., without any restrictions to the type of coupling that one considers).

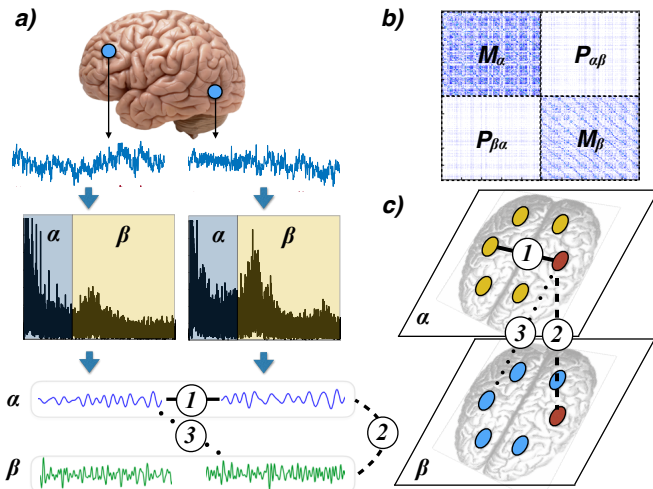


FIG. 1: Encoding brain dynamics as a multilayer functional network. Qualitative example with two frequency bands (alpha and beta). (a) The MEG signals are band-pass filtered at two frequency bands: alpha [8–12] Hz and beta [12–30] Hz. We use mutual information (MI) [29] to quantify the coordination between brain regions. This yields three different type of functional edges: edge “1” quantifies the coordination between different regions at the same frequency band; edge “2” corresponds to interlayer edges, which couple the activity of the same region at different frequency bands; and edge “3” quantifies the cross-frequency coupling between different brain regions. Multiplex networks include only edges of types (1) and (2), whereas more general multilayer networks include all three types of edges. (b) Schematic of the supra-adjacency matrix of a 2-layer network constructed from the data in panel (a). (c) Schematic of the intralayer and interlayer edges in the multilayer functional network.

RESULTS

Obtaining frequency-based multilayer networks

In Fig. 1, we illustrate the process of constructing frequency-based multiplex and multilayer brain networks. Our starting point is a data set of MEG recordings of a group of 89 individuals during resting state (see Materials and Methods for details), but other experimental paradigms — including different brain imaging techniques such as fMRI or EEG — can be used to construct multilayer networks with the same procedure. Specifically, we record MEG activity at $N \approx 250$ cortical regions and then clean it to remove artifacts to obtain corresponding unfiltered signals. In this way, we analyze the signal recorded by each sensor instead of carrying out a source reconstruction. We then band-pass filter each signal to obtain four different filtered time series for each brain region. We use the four classical frequency bands: theta [3–8] Hz, alpha [8–12] Hz, beta [12–30] Hz, and gamma [30–100] Hz. The number l of layers of the multilayer network is the number of different frequencies in which we are interested (so $2 \leq l \leq 4$ in this case),

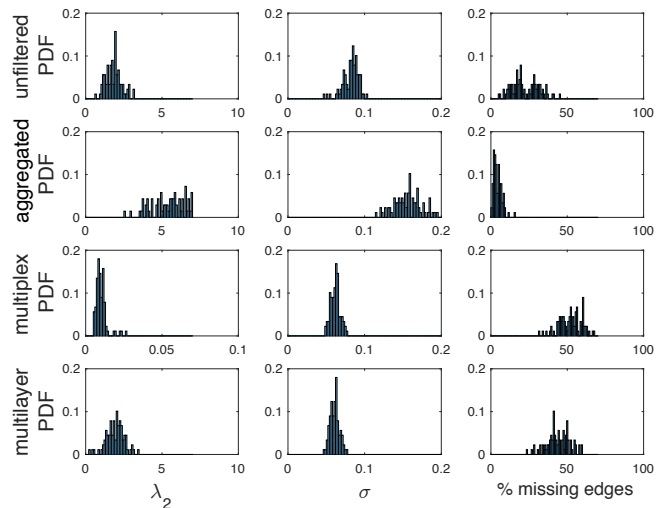


FIG. 2: MEG data sets: From unfiltered data to a multilayer network. Probability distribution functions (PDFs) of different network characteristics of a group of 89 individuals (see Materials and Methods for details). We show the second-smallest eigenvalue λ_2 of the combinatorial Laplacian matrix, the standard deviation σ of the matrix elements (to quantify their heterogeneity), and the percentage of missing edges of four different networks: (i) the functional network obtained from the unfiltered signals (first row), (ii) an aggregated network of the alpha and beta layers (second row), (iii) a multiplex network (third row), and a (iv) full multilayer network (fourth row). In all cases, we only consider two layers (alpha and beta). The percentage of missing edges in the unfiltered and aggregated networks is equal to the percentage of zeros in the whole matrix, but it refers only to the interlayer edges for the multiplex and multilayer networks.

and the N nodes in each layer are associated with the dynamics of the N sensors filtered at its corresponding frequency band. We number the nodes such as nodes n , $n + N$, $n + 2N$, \dots , $n + lN$ (with $n \in \{1, \dots, N\}$) correspond to the signals of the same brain region n at the l different frequency bands (i.e., layers).

We now quantify the coordination between any pair of nodes of a multilayer network, regardless of which layers they are in, using mutual information MI (see Materials and Methods). Calculating MI between time series of the same frequency band yields intralayer connections between brain regions (see edge “1” in the bottom left plot of Fig. 1a for an example), so each layer corresponds to a specific frequency band. Edges between the signals of the same sensor but at different frequency bands result in interlayer connections between layers (see edge “2”). Such “diagonal” interlayer edges are the only type of interlayer edges that are allowed in multiplex networks [1]. Finally, cross-frequency coupling between different brain regions yield the other (“non-diagonal”) interlayer edges in a full multilayer network (see edge “3”). As we show in Fig. 1(b), we thereby obtain a supra-adjacency matrix, where blocks along the diagonal account for the intralayer connections (layers alpha and beta in the 2-layer exam-

| Network | σ | missing edges |
|-------------------|----------|---------------|
| unfiltered | 0.0823 | 22.75% |
| aggregated | 0.1567 | 4.42% |
| multiplex | 0.0618 | 52.17% |
| (full) multilayer | 0.0611 | 44.01% |

TABLE I: For each kind of network (see first column): standard deviation σ of the weight of the edges (unfiltered and aggregated) and interlayer edges (for both multiplex networks and full multilayer networks) and the corresponding percentage of missing edges.

ple), and blocks off of the diagonal, marked as $\mathbf{P}_{\alpha\beta}$ and $\mathbf{P}_{\beta\alpha}$, contain the interlayer edges. Because $MI_{ij} = MI_{ji}$, the supra-adjacency matrix is symmetric, so $\mathbf{P}_{\alpha\beta} = \mathbf{P}_{\beta\alpha}^T$.

Importantly, although we have chosen to use MI, there are a diversity of similarity measures for capturing amplitude–amplitude and phase–amplitude correlations between different frequency bands (see [30] for a review on cross-frequency coupling measures), and each measure has its own advantages and drawbacks. Nevertheless, as we will see, the same methodological implications exist no matter which specific measure one uses to evaluate coordination between brain sites.

In our discussion, we focus on the analysis of a 2-layer network with alpha and beta layers, and we will discuss the consequences of considering alternative frequency bands and numbers of layers in the last section of the paper.

Our starting point is to compare the results from four different constructions of functional networks:

- (i) *Unfiltered functional networks.* We obtain these networks from the original (unfiltered) signals of each brain region — i.e., without decomposing the signals into different frequency bands — so these are monolayer networks.
- (ii) *Aggregated networks.* We obtain these networks from componentwise addition of the weights of the alpha and beta layers to form monolayer networks.
- (iii) *Multiplex networks,* where each layer corresponds to a specific frequency band (as explained above) and interlayer edges are allowed only between nodes corresponding to the same brain region.
- (iv) *Full multilayer networks,* which include the same layers as their multiplex counterparts, but with all possible interlayer edges.

In Fig. 2, we show probability distribution functions (PDFs) for the group of 89 individuals of the values of λ_2 , specifically, the standard deviation of the interlayer edge weights (to quantify their heterogeneity), and the percentage of missing interlayer edges (see also Table I).

In Fig. 2 (first column), we observe that the (monolayer) unfiltered functional network has similar a mean

and standard deviation of λ_2 as the multilayer one (see also Table I). However, the aggregated networks tender to have larger values of λ_2 , which makes sense, as we construct such a network by adding the weights of the two layers (alpha and beta), and the total “strength” of the network (i.e., sum of all of its edge weights) is close to the double the strength of each layer. Importantly, the mean λ_2 for the multiplex networks is two orders of magnitude small than the mean λ_2 of the multilayer networks. We expect this discrepancy, because we construct a multiplex network by deleting all interlayer edges of a full multilayer network, exception for ones (so-called “diagonal” edges) that link the same “physical” nodes. Thus, the total strength of the interlayer matrix $\mathbf{P}_{\alpha\beta}$ is considerably smaller in multiplex networks than in corresponding full multilayer networks. Because λ_2 is an indicator of the amount of interconnections between communities in a network [24], one expects such drastic edge removals to yield a lower value of λ_2 , as layers can be construed as communities with a small number of edges between them (only N of the N^2 possible interlayer edges of the full multilayer network).

In columns two and three of Fig. 2, we quantify the heterogeneity and the number of missing interlayer edges of the four different functional networks. In column two, we plot the PDFs of the standard deviation of all edges (unfiltered and aggregated networks) and interlayer edges (multiplex and multilayer networks). In all cases, we observe that the functional networks obtained from the experimental data sets have a non-negligible heterogeneity (see also Table I). Again, aggregated networks have values that are roughly double those of the other kinds of networks because of the (rough) doubling of the mean strength. Finally, in column three, we show that the thresholding process that removes connections that are not statistically significant leads to a high percentage of missing edges. (See Materials and Methods for details.) The (monolayer) aggregated networks have the lowest mean percentage, followed by the (monolayer) unfiltered networks, and then the two types of multilayer networks. For the multiplex and full multilayer networks, the percentage of missing edges, which is higher than 40% in both cases, refers to the number of all possible interlayer edges. Note that missing edges are unavoidable in functional brain networks, because not all brain regions communicate with each other through direct connections [41]. Moreover, the different amounts of coordination between brain sites lead to functional networks with heterogeneous weights.

Heterogeneity and missing interlayer edges in multiplex networks

Given our prior observations, a crucial question arises: What are the consequences of heterogeneity and missing interlayer edges, both intrinsic features of brain imaging data sets, on multiplex and full multilayer functional

networks? More specifically, how do they affect the value of λ_2 (and hence structural and dynamical implications that arise from such differences)?

With the aim of answering both questions, we do a series of numerical simulations in which we compare the theoretical values of λ_2 in multiplex and full multilayer networks from homogeneous interlayer-edge distributions with ones from networks with heterogeneous and missing interlayer edges.

We start with a 2-layer multiplex network, whose layers alpha and beta have $N_\alpha = N_\beta$ nodes and $L_\alpha = L_\beta$ intralayer edges, respectively. We number the nodes of layer alpha from $k = 1$ to $k = N_\alpha$ and the nodes of layer beta from $l = N_\alpha + 1$ to $l = N_{\alpha\beta} = N_\alpha + N_\beta$. The matrices \mathbf{M}_α and \mathbf{M}_β are the corresponding adjacency matrices for each layer. We then introduce L_c connector edges (i.e., diagonal interlayer edges) between each node k of layer alpha to its corresponding node $l = k + N_\alpha$ of layer beta to construct a multiplex network. We suppose that intralayer edges have weight $w_{ij}^{\text{intra}} = 1$ (i.e., for i and j belonging to either to layer alpha or to layer beta), and we set the weight of the interlayer edges to $w_{kl}^{\text{inter}} = p_{kl}$ (i.e., for $k \in \alpha$ and $l \in \beta$), where p_{kl} are the elements of a vector \vec{p} containing the weights of the interlayer connections. Under these conditions, we obtain a supra-adjacency matrix $\mathbf{M}_{\alpha\beta}$, which consists of two diagonal blocks (\mathbf{M}_α and \mathbf{M}_β) and two off-diagonal blocks ($\mathbf{P}_{\alpha\beta}$ and $\mathbf{P}_{\beta\alpha}$, where $\mathbf{P}_{\alpha\beta} = \mathbf{P}_{\beta\alpha}^T = \vec{p}\mathbb{I}$, where \vec{p} is a row vector). That is,

$$\mathbf{M}_{\alpha\beta} = \begin{pmatrix} \mathbf{M}_\alpha & \vec{p}\mathbb{I} \\ \vec{p}\mathbb{I} & \mathbf{M}_\beta \end{pmatrix}, \quad (1)$$

where \mathbb{I} is an identity matrix.

The combinatorial supra-Laplacian matrix $\mathcal{L}_{\alpha\beta}$ of the multiplex network is

$$\mathcal{L}_{\alpha\beta} = \begin{pmatrix} \mathcal{L}_\alpha + \vec{p}\mathbb{I} & -\vec{p}\mathbb{I} \\ -\vec{p}\mathbb{I} & \mathcal{L}_\beta + \vec{p}\mathbb{I} \end{pmatrix}, \quad (2)$$

where the layer combinatorial Laplacians $\mathcal{L}_{\alpha,\beta}$ are

$$\mathcal{L}_{\alpha,\beta}(i, j) = \begin{cases} s_i, & \text{if } i = j \\ -1, & \text{if } i \text{ and } j \text{ are connected} \\ 0, & \text{otherwise} \end{cases}, \quad (3)$$

and $s_i = \sum_{i \neq j} w_{ij}$ is the weighted degree (i.e., total weight of incident edges) of node i .

In Fig. 3, we show the consequences of heterogeneity on the distribution of the weights of interlayer edges of the multiplex network $\mathbf{M}_{\alpha\beta}$. In this example, the multiplex network has an interlayer connection matrix $\mathbf{P}_{\alpha\beta} = \vec{p}\mathbb{I}$, where \mathbb{I} is an $N_\alpha \times N_\alpha$ (equivalently, $N_\beta \times N_\beta$, as $N_\alpha = N_\beta$ in this example) identity matrix and $\vec{p} = p\vec{h}$ is a row vector controlling the weights of interlayer edges, where p modulates its amplitude and the vector \vec{h} encodes the heterogeneity of the interlayer edges. We set

the elements of \vec{h} to follow a uniform distribution over the interval $[h_{\min}, h_{\max}]$. These elements have a mean value of \bar{h} and a standard deviation of σ . We set $\bar{h} = 1$ and create networks with interlayer-edge-weight heterogeneities that range from $\sigma = 0$ (blue circles) to $\sigma \approx 0.581$ (green circles). We then analyze the interplay between the weights of the interlayer edges and the heterogeneity by increasing the value of p . Note that $\sigma = 0$ corresponds to what we call a *homogeneous multiplex network*, which has uniformly-weighted interlayer edges (i.e., $\vec{p} = p$ for all i and j). We obtain the results in Fig. 3 from a mean over 100 realizations of 2-layer networks with the Erdős-Rényi (ER) model ($p_{\text{con}} = 0.25$) in each layer and $N_\alpha = N_\beta = 250$ nodes [31].

As explained in [4], modifying the weight parameter p of the interlayer edges has important consequences for the value of λ_2 of homogeneous multiplex networks. The existence of two regimes of qualitatively distinct dynamics, separated at a transition point p^* , was discussed in [4] (and in various subsequent papers): when $p \ll p^*$, the algebraic connectivity λ_2 follows the linear relation $\lambda_2 = 2p$; for $p \gg p^*$, the value of λ_2 approximates that of the aggregated network [i.e., $\lambda_{2,\text{agg}} = \frac{1}{2}\lambda_2(\mathcal{L}_\alpha + \mathcal{L}_\beta)$]. In Fig. 3, the dashed and solid lines indicate the theoretical predictions of λ_2 in the homogeneous case for low (dashed) and high (solid) values of p . We obtain a mean value of $p^* \approx 2.870$ by locating the intersection between the eigenvalues λ_2 and λ_3 of the supra-Laplacian matrix $\mathcal{L}_{\alpha\beta}$ [32].

Interestingly, Fig. 3(a) shows that the heterogeneity of the interlayer edges leads to non-negligible differences of λ_2 . Furthermore, values of p near p^* show the maximum discrepancy between the heterogeneous case (colored circles) and the homogeneous case (black circles). These results suggest that assuming the same weight p for all interlayer edges in real networks will lead to unavoidable errors in the estimation of λ_2 , especially near the transition point p^* .

Deviations from the expected value of λ_2 increase even further when a certain number of interlayer edges is missing. In Fig. 3(b), we show the effects of removing some percentage of the interlayer edges in a “holey” multiplex network (i.e., a multiplex network with an interlayer matrix $\mathbf{P}_{\alpha\beta}$ whose elements are either 1 or 0 in the diagonal and 0 in all other elements). We observe that increasing the number of missing interlayer edges causes the multiplex networks to have drastically reduced values of λ_2 . When $p \ll p^*$, the value of λ_2 always grows with a slope that is smaller than $2p$; for $p \gg p^*$, the value of λ_2 never reaches the value of λ_2 for the aggregated network. Finally, values of p close to p^* again have the largest discrepancies with the homogeneous case.

Multiplex networks versus full multilayer networks

We now identify the qualitative differences (and some of their consequences) between multiplex networks and

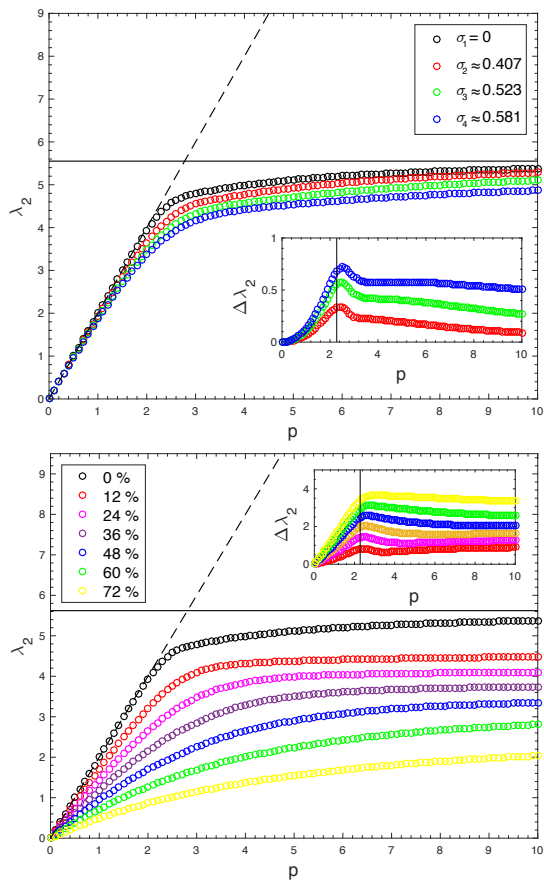


FIG. 3: Consequences of heterogeneity and missing interlayer edges in a multiplex network. Algebraic connectivity λ_2 of the combinatorial supra-Laplacian matrix $\mathcal{L}_{\alpha\beta}$. Each of the two layers is an Erdős-Rényi network with $N = 250$ nodes and a connection probability of $p_{\text{con}} = 0.25$. Circles correspond to means over 100 realizations. **(a)** We quantify the heterogeneity of the interlayer edges by the standard deviation σ of their weights: (i) $\sigma = 0$ (black circles), (ii) $\sigma \approx 0.407$ (red circles), (iii) $\sigma \approx 0.523$ (green circles), and (iv) $\sigma \approx 0.581$ (blue circles). Lines correspond to the two analytical solutions for the case $\sigma = 0$ (i.e., a homogeneous multiplex network). The dashed line is $\lambda_2 = 2p$, and the solid line is $\lambda_{2,\text{agg}} = \frac{1}{2}\lambda_2(\mathcal{L}_\alpha + \mathcal{L}_\beta)$ [4, 32]. Inset: $\Delta\lambda_2$ is the difference of λ_2 between the homogeneous multiplex network and multiplex networks with heterogeneous interlayer edges. **(b)** Algebraic connectivity λ_2 of the multiplex network as a function of the number of missing interlayer edges. Inset: $\Delta\lambda_2$ is the difference of λ_2 between the homogeneous multiplex network (i.e., $\sigma = 0$ and all possible interlayer edges) and the multiplex networks with missing interlayer edges. The solid vertical line indicates the mean value of p^* .

full multilayer networks, where the latter have an interlayer connectivity matrix of $\mathbf{P}_{\alpha\beta} = p\mathbf{C}$, where the matrix \mathbf{C} has elements c_{ij} that account for the weight between each pair of nodes $i \in \alpha$ and $j \in \beta$, and the parameter p allows one to modulate the mean weight of the interlayer edges. In Fig. 4(a), we connect the same layers as in the previous section, but now we use a homogeneous

interlayer connectivity matrix $\mathbf{P}_{\alpha\beta}$ with weights $p_{ij} = p$ (i.e., $c_{ij} = 1$ for all i and j). Increasing from 0 the value of p leads to the transition point $p^* \approx 0.013$, which we obtain from the intersection of the eigenvalues λ_2 and λ_3 of the combinatorial supra-Laplacian $\mathcal{L}_{\alpha\beta}$. We observe for $p < p^*$ that the value of λ_2 follows the linear function $\lambda_2 = 2p\langle c \rangle$ (dashed line of Fig. 4(a)), where $\langle c \rangle = 250$ is the mean weighted degree of the matrix \mathbf{C} , as demonstrated in [4]. Interestingly, after the transition point $p = p^*$, the value of λ_2 can be described by the function $\lambda_2 = \lambda_{2,\min(\alpha,\beta)} + \lambda_2(p\mathbf{C})$, where $\lambda_{2,\min(\alpha,\beta)}$ is the value of the smaller λ_2 of the two isolated layers. As we show in the inset of Fig. 4(a), when a certain amount of heterogeneity is introduced into the interlayer connectivity matrix, we observe differences with the homogeneous case, but they are only significant for values of p larger than the transition point $p = p^*$.

As we observed in the analogous scenario for multiplex networks, deleting interlayer edges of a full multilayer network increases the differences of λ_2 with that of a homogeneous multilayer network. As we show in Fig. 4(b), the value of λ_2 decreases with the number of missing edges, which one may expect, because having a smaller number of interlayer edges implies that one needs larger connection weights to maintain the same amount of interlayer coupling. Interestingly, the deviation from the theoretical predictions is significant even for $p < p^*$. Additionally, for $p > p^*$, we observe the expected change in the slope of λ_2 , but the theoretical predictions given by $\lambda_2 = \lambda_{2,\min(\alpha,\beta)} + \lambda_2(p\mathbf{C})$ (solid line) begin to fail, leading to a discrepancy that increases with the number of missing edges.

Because full multilayer networks have up to N^2 interlayer edges, whereas multiplex networks can have only N of them, the former tend to have interlayer connectivity matrices with higher strengths $S_P = \sum_{ij} p_{ij}$. In Fig. 5, we show the algebraic connectivity λ_2 of the combinatorial supra-Laplacian matrix $\mathcal{L}_{\alpha\beta}$ for a series of networks with identical layers and interlayer strength S_P , but with a different number of interlayer edges, ranging from a multiplex network (N interlayer edges) to a full multilayer network with no nonzero entries (N^2 interlayer edges). The dashed lines correspond to the analytical solutions for the full multilayer network (black dashed line; $\lambda_2 = 2p\langle c \rangle$, with $\langle c \rangle = 250$) and the multiplex network (red dashed line; $\lambda_2 = 2p$) when $p < p^*$. The solid lines are the corresponding theoretical solutions when $p > p^*$ for the full multilayer network (black line; $\lambda_2 = \lambda_{2,\min(\alpha,\beta)} + \lambda_2(p\mathbf{C})$) and the multiplex network (red line; $\lambda_{2,\text{agg}} = \frac{1}{2}\lambda_2(\mathcal{L}_A + \mathcal{L}_B)$). We observe the effect that adding interlayer edges to multiplex networks has on the value of λ_2 and the associated transition from a multiplex network to a full multilayer architecture. Interestingly, the different numbers of interlayer edges in the two types of networks leads to a difference in the position of p^* (which can be inferred by looking at the change of slope of λ_2) that can reach several orders of magnitude.

The inset of Fig. 5 shows the same results normalized

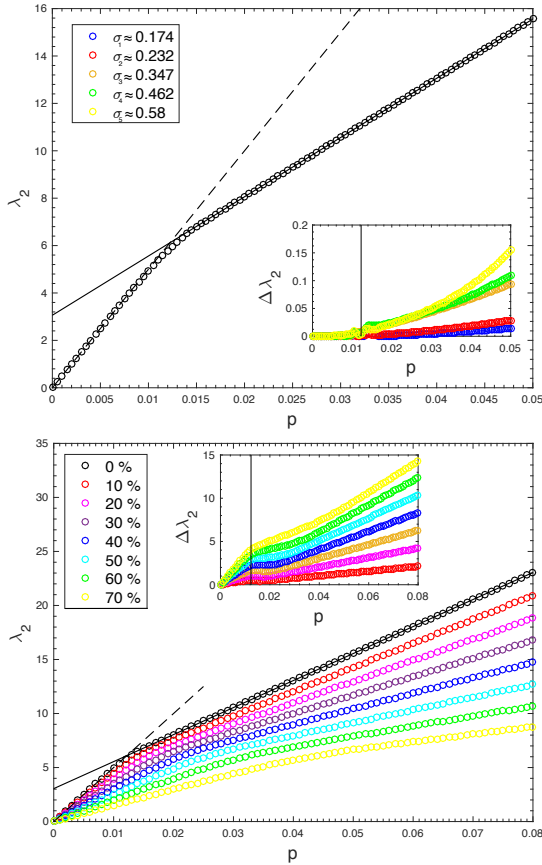


FIG. 4: **Edge heterogeneity and missing interlayer edges in a full multilayer network.** Algebraic connectivity λ_2 of the combinatorial supra-Laplacian matrix $\mathcal{L}_{\alpha\beta}$ (black circles) as a function of the weight parameter p of the interlayer connections. Each of the two layers is an Erdős-Rényi network of $N = 250$ nodes with a connection probability $p_{\text{con}} = 0.25$. Circles are the mean over 100 realization of such multilayer networks. **(a)** Algebraic connectivity λ_2 for a homogeneous interlayer connectivity matrix $\mathbf{P}_{\alpha\beta} = p\mathbf{C}$, where each of the elements of \mathbf{C} is $c_{ij} = 1$. The dashed line, given by $\lambda_2 = 2p\langle c \rangle$, corresponds to the analytical solution for a homogeneous matrix $\mathbf{P}_{\alpha\beta}$, where \mathbf{C} has a mean weighted degree of $\langle c \rangle = 250$. The solid line is given by $\lambda_2 = \lambda_{2,\min(\alpha,\beta)} + \lambda_2(p\mathbf{C})$, where $\lambda_{2,\min(\alpha,\beta)}$ is the value of the smaller λ_2 of the two isolated layers. The inset shows the differences $\Delta\lambda_2$ between a multilayer network with homogeneous interlayer connectivity matrix $\mathbf{P}_{\alpha\beta}$ and a series of multilayer networks with an increasing heterogeneity in $\mathbf{P}_{\alpha\beta}$ (quantified by the standard deviation σ). Differences with the homogeneous case increase after the critical point (p^*) (vertical solid line). **(b)** Algebraic connectivity λ_2 of the full multilayer network as a function of the percentage of missing interlayer edges (see the figure legend). Inset: Increment of λ_2 versus the number of missing interlayer edges.

with the percentage of strength of the interlayer connectivity matrix. That is, we show $S_P/(S_\alpha + S_\beta)$, where $S_\alpha = \sum M_{\alpha,ij}$ and $S_\beta = \sum M_{\beta,ij}$, respectively, are the strengths of layers alpha and beta. This allows us to compare networks with the same S_P , regardless of whether

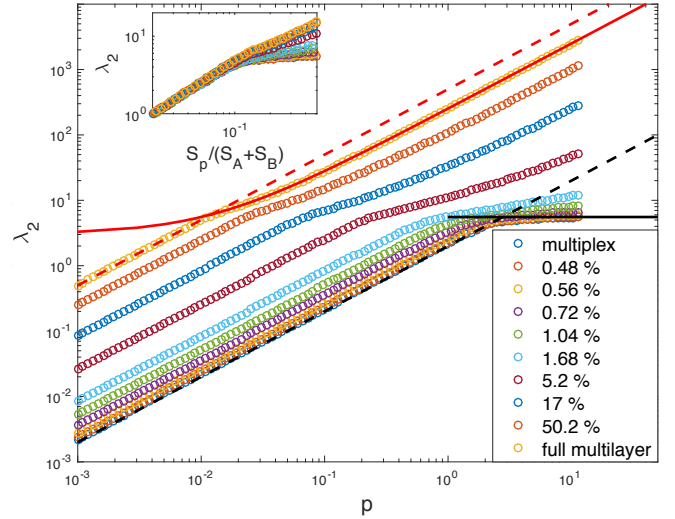


FIG. 5: **Transition from a multiplex network to a full multilayer network.** Algebraic connectivity λ_2 of the combinatorial supra-Laplacian matrix $\mathcal{L}_{\alpha\beta}$ for different values of the percentage of edges in the interlayer connectivity matrix $\mathbf{P}_{\alpha\beta}$. Departing from a multiplex network, we add interlayer edges at uniformly at random and calculate the percentage of existing edges in $\mathbf{P}_{\alpha\beta}$. Each circle corresponds to the mean over 100 realizations. We set all active edges of the interlayer connectivity matrix $\mathbf{P}_{\alpha\beta}$ to $p_{ij} = p$. The dashed lines correspond to the analytical solutions for the full multilayer network (black dashed line; $\lambda_2 = 2p\langle c \rangle$, with $\langle c \rangle = 250$) and the multiplex network (red dashed line; $\lambda_2 = 2p$) for $p < p^*$. The solid lines are the theoretical solutions when $p > p^*$ for the full multilayer network (black line; $\lambda_2 = \lambda_{2,\min(\alpha,\beta)} + \lambda_2(p\mathbf{C})$) and the multiplex network (red line; $\lambda_{2,\text{agg}} = \frac{1}{2}\lambda_2(\mathcal{L}_A + \mathcal{L}_B)$). Inset: λ_2 versus $S_P/(S_\alpha + S_\beta)$, where S_P , S_α , and S_β are, respectively, the strength of the interlayer matrix $\mathbf{P}_{\alpha\beta}$, the strength of layer alpha, and the strength of layer beta. Note that differences between the value of λ_2 of the multilayer structures increase significantly for $S_P/(S_\alpha + S_\beta) \gtrsim 0.1$.

they are close to a multiplex architecture or to a fully multilayer architecture with no nonzero entries. Below the transition point p^* , we obtain similar values of λ_2 for all network architectures. It is only for $p > p^*$ that the particular structure of the interlayer connectivity matrix begins to play a role in the value of λ_2 . We observe that differences start to arise at $S_P/(S_\alpha + S_\beta) \approx 0.1$, which is a relatively low value.

Although we used ER intralayer networks in our analysis above, we obtain similar results for other network models. In particular, the results are qualitatively the same when we construct the intralayer networks using a Barabási-Albert (BA) model [33]. (See the Supplementary Information for details.)

The meaning of λ_2 in experimental data

Now that we have analyzed the effect of the heterogeneity and the number of missing interlayer edges, let's

revisit the multiplex and multilayer networks obtained from the MEG recordings. As we saw in Fig. 2, both edge-weight heterogeneity and missing interlayer edges occur in our experimental data, and it is thus desirable to investigate how close our networks constructed from experimental data are to a transition point p^* and how this proximity (or lack thereof) influences the expected value of λ_2 .

In Fig. 6, we show the values of λ_2 that we obtain for four different network reconstructions based on the MEG data: a homogeneous multiplex network (black circles), a heterogeneous multiplex network (red circles), a homogeneous full multilayer network (blue circles), and a heterogeneous full multilayer (cyan circles). Each networks has two layers — one for the alpha band and one for the beta band — and each point corresponds to the mean over the group of 89 individuals. First, we obtain the heterogeneous versions of the multiplex and multilayer networks from the *MI* values between the brain regions in frequency bands as described in the previous sections (see also Materials and Methods). Second, we construct the homogeneous versions of both the multiplex and multilayer networks by assigning the same weight $\langle c \rangle$ to all interlayer edges, where $\langle c \rangle$ is the mean of the weights of the interlayer edges in their heterogeneous counterparts. Note that, in this case, the homogeneous multiplex and multilayer networks do not correspond to real functional networks, but instead they are a reference to quantify the consequences on λ_2 of the intrinsic heterogeneity and missing edges in real functional networks. To assess how close the real networks are to the transition point p^* , we multiply the value of the interlayer edges by a parameter p , which we increase from $p = 0$ to $p > 1$. We then calculate the strength S_P of the corresponding interlayer connectivity matrix $\mathbf{P}_{\alpha\beta}$ to allow a comparison between the multiplex network and the multilayer networks, and we then plot the value of λ_2 versus S_P . The red dashed line in Fig. 6 corresponds to the theoretical predictions for $p < p^*$ (i.e., $\lambda_2 = 2p\langle c \rangle$, where $\langle c \rangle$ is the mean weighted degree of the nodes in the interlayer connection matrix $\mathbf{P}_{\alpha\beta}$). The black and blue dashed lines are, respectively, the value of λ_2 for the aggregated network divided by 2 [i.e., $\lambda_{2,\text{agg}} = \frac{1}{2}\lambda_2(\mathcal{L}_\alpha + \mathcal{L}_\beta)$] and the value of λ_2 for the unfiltered (monolayer) functional network. The vertical solid line corresponds to the case of $p = 1$ for the mean of the heterogeneous full multilayers networks (i.e., the networks that we obtain by taking into account all interlayer correlations without modifying their weights). Interestingly, this network occupies the region in which the evolution of λ_2 with respect to p is changing slope from $\lambda_2 = 2p\langle c \rangle$ to $\lambda_2 = \lambda_{2,\min(\alpha,\beta)} + \lambda_2(p\mathbf{C})$, which suggests that the frequency-based multilayer networks that we analyze are close to the transition point p^* . As we have seen, it is near this point where the value of λ_2 is most influenced by the effects of heterogeneity and missing interlayer edges. It is also worth noting that none of the other three network representations give accurate approximations to the algebraic connectivity (and hence,

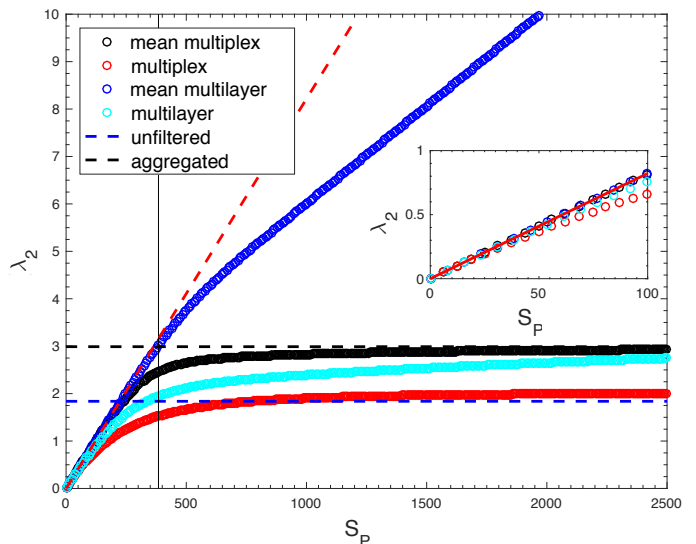


FIG. 6: Edge heterogeneity and missing interlayer edges in frequency-based functional brain networks. Algebraic connectivity λ_2 of the combinatorial supra-Laplacian matrix $\mathcal{L}_{\alpha\beta}$ as a function of the mean strength of the interlayer connectivity matrix $\mathbf{P}_{\alpha\beta} = p\mathbf{C}$, where \mathbf{C} encodes the weights of the interlayer edges, for four different types of networks: (i) homogeneous multiplex networks, (ii) heterogeneous multiplex networks, (iii) homogeneous full multilayer networks, and (iv) heterogeneous full multilayer networks. Circles are means over 89 individuals. The blue and black dashed lines, respectively, are the values of λ_2 for the unfiltered and aggregated networks. The red dashed line corresponds to $\lambda_2 = 2p\langle c \rangle$, where $\langle c \rangle$ is the mean of the weighted degree. The red solid line is given by $\lambda_2 = \lambda_{2,\min(\alpha,\beta)} + \lambda_2(p\mathbf{C})$, where $\lambda_{2,\min(\alpha,\beta)}$ is the value of the smaller λ_2 of the two isolated layers. The inset shows a magnification for low values of p .

we expect, of spectral properties more generally) of the heterogeneous multilayer network, unless we are in the region in which $p \ll p^*$. (See the inset of Fig. 6.)

This fact can be observed in more detail in Fig. 7, where we show (top panel) the PDF of the values of p^* calculated for each of the 89 individuals and (bottom panel) the percentage of deviation of λ_2 with respect to the value in the aggregated network $\lambda_{2,\text{agg}}$. Observe that the peak of the PDF for p^* is near $p = 1$. Moreover, this figure confirms that the aggregated network is not an accurate estimator of λ_2 for the multilayer networks, and there is not even a clear correlation with the value of p^* , thus making necessary for spectral analyses to consider the heterogeneous, full multilayer networks.

Finally, we investigate how the combination of layers from different frequency bands affects the value of λ_2 . In our analysis thus far, we have focused on the 2-layer network formed by alpha and beta frequency bands, because they are often associated to brain activity during the resting state. Nevertheless, because the signal has been filtered into $l = 4$ different frequency bands, there are 8 possible combinations of 2 layers. In Fig. 8, we show

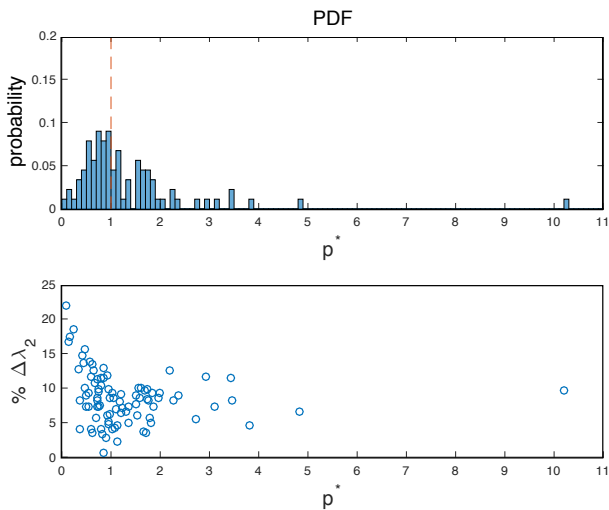


FIG. 7: **MEG of full multilayer networks and the transition point p^* .** (Top) Probability distribution function (PDF) of the transition point p^* for the 2-layer networks (containing the alpha and beta layers) of the 89 individuals. The dashed line corresponds to $p^* = 1$. (Bottom) Percentage of deviation of λ_2 with respect to the value of the aggregated network: $\% \Delta \lambda_2 = (\lambda_{2,\text{agg}} - \lambda_2) / \lambda_{2,\text{agg}}$, where λ_2 is the algebraic connectivity of full multilayer networks of the 89 individuals.

| Layer | intralayer strength | interlayer strength |
|--------------------|---------------------|---------------------|
| theta (θ) | 12.69% | 9.53% |
| alpha (α) | 31.43% | 7.49% |
| beta (β) | 12.18% | 9.34% |
| gamma (γ) | 6.85% | 10.47% |

TABLE II: **Percentage of strength of each layer in the (4-layer) multilayer network.** The first column indicates the layer. The second column indicates the percentage of strength of all intralayer edges in the full 4-layer multilayer network that come from that layer; that is, for a layer m , the percentage is given by $100 \times \frac{M_m}{M_{\theta\alpha\beta\gamma}}$. The third column gives the percentage of the strength of the interlayer edges; that is, for a layer m , the percentage is $100 \times \frac{\sum_{m \neq l} P_{ml}}{M_{\theta\alpha\beta\gamma}}$, where $l = \theta, \alpha, \beta, \gamma$.

the relation between λ_2 for all possible combinations of 2-layer networks versus the full 4-layer multilayer. Observe the strong correlation of the 2-layer networks that include the gamma layer (especially the one that is composed of theta and gamma layers) with the full multilayer network. One can explain such a correlation by inspecting the total strength of each frequency band. In Table II, we separate the intralayer and interlayer strengths to facilitate interpretation of the results. We observe that gamma is the least active layer, as it is the one with the lowest intralayer strength. Nevertheless, it has the highest interlayer strength, so it is the layer that appears to interact most strongly with the other layers. Because, as we have seen, the full multilayer functional networks are

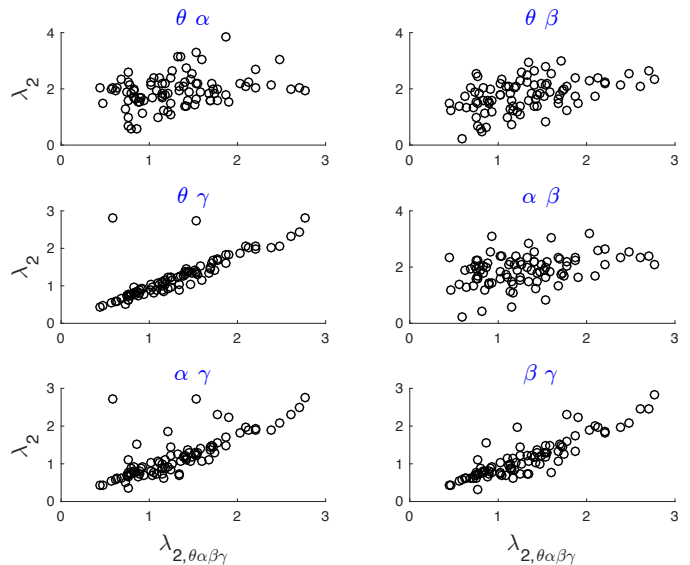


FIG. 8: **Combining different frequency bands into multilayer networks.** Algebraic connectivity λ_2 of all possible combinations of 2-layer networks versus $\lambda_{2,\theta\alpha\beta\gamma}$ of the 4-layer full multilayer networks, with layers theta (θ), alpha (α), beta (β), and gamma (γ). The labels at the top of each plot correspond to the frequency bands that we use to construct the layers. Each circle corresponds to one of the 89 individuals.

close to the transition point, the weight of the intralayer connections has a strong influence on the value of λ_2 . Therefore, the theta-gamma (2-layer) network, which includes layers with the highest interlayer strengths, is the one with the strongest correlation of λ_2 with the full multilayer network [see Fig. 8(c)].

Conclusions

Using network analysis as a tool for analyzing brain-imaging data and, more specifically, implementing a multilayer description of brain activity has both advantages and drawbacks that must be investigated carefully. As we have discussed, it is possible to encode such information as either a multiplex network or as more general types of multilayer networks, but different choices lead to different results, which must then be interpreted from a neuroscientific perspective. In our paper, we have performed such an analysis to explore the implications of the two approaches on spectral information, and in particular the algebraic connectivity λ_2 , which has been related to structural, diffusion, and synchronization properties of networks [4, 7, 28]. Specifically, we have seen how the heterogeneity of the interlayer edges of multiplex networks leads to deviations of the theoretical predictions obtained when all interlayer edges have an equal weight p , and we observed that the deviation is even larger when interlayer edges are missing. The importance of these results, which imply large differences in qualitative dynamics, is under-

scored by the fact that both heterogeneity and missing interlayer edges are common features for brain-imaging data.

It is also important to understand that representing brain activity as a multiplex network rather than a full multilayer network has important conceptual drawbacks: (i) each brain region does not necessarily coordinate with itself at different frequencies; and (ii) there may also exist cross-frequency coupling between different brain regions. Consequently, interlayer connections do not necessarily follow the multiplex paradigm, because some of the interlayer edges probably should not be present that others, to account for interlayer coupling between different nodes (i.e., different brain regions), should be included, thus requiring a fully general multilayer approach.

Our numerical simulations with full multilayer networks show that the value of λ_2 differs dramatically from that for multiplex networks. This makes sense, because the number of interlayer edges scales with N in the multiplex networks but with N^2 in the multilayer networks, leading to important quantitative differences in the values of the algebraic connectivity. Nevertheless, the effects of heterogeneity and missing interlayer edges on full multilayer networks are qualitatively similar to those obtained with multiplex networks. Specifically, the analytical predictions that we obtained with homogeneous multilayer networks deviate from those of heterogeneous cases, showing an important discrepancy for values of the coupling-strength parameter p larger than the transition point p^* . Again, the effect of missing interlayer edges is particularly dramatic once the value of p^* is reached.

Our analysis of experimental imaging data confirms our results with synthetic networks. The small number of interlayer connections in a multiplex network leaves the system in a region in layers behave as if they are structurally independent, and a deeper analysis reveals that the weights of the interlayer edges from the experimental data need to be increased by several orders of magnitude to reach the transition point p^* . Consequently, using a multiplex representation leads to a network with structurally independent layers, unless unrealistic weights (i.e., $p \gg 1$) are assigned to the interlayer edges.

Interestingly, this pathology does not occur when one uses a full multilayer description, in which a frequency band from one brain region is now allowed to couple with a different frequency band from a different brain region. When one considers all possible interlayer edges, the majority of the 89 individuals in the experiment are close to the transition point p^* , even though the percentage of weight in the interlayer edges is always around 10% of that of the intralayer ones (see Table II). As we showed by in our computations with synthetic data, it is around this point that heterogeneity and missing interlayer edges begin to yield important discrepancies with the theoretical results from homogeneous multilayer networks [see Fig. 4(a)].

Note that the percentage of weight of interlayer edges

depends strongly on how one measures coordination between brain regions. When one uses diagnostics other than mutual information, it is possible to observe differences in this percentage, which may move multilayer networks above or below the transition point. Thus, no matter what measure one uses, it is mandatory to first analyze the percentage of weight in the interlayer edges and to interpret the value of λ_2 with respect to the value of p^* .

The fact that, in frequency-based multilayer networks, the weight of interlayer edges strongly influences the value of λ_2 despite being much smaller than the weights of intralayer edges (see Table II) highlights the importance of adequately evaluating cross-frequency coupling, which has traditionally been disregarded when representing brain activity in terms functional networks. As has been discussed prominently in neuroscience (including in critiques of connectomics) [34], the dynamics matter, and that necessarily must include incorporation and analysis of coupling between different frequency bands. Moreover, the methodology that is used to quantify interaction between brain regions at different frequencies lead to different values of λ_2 , and there are also other important dynamical issues, such as phase-amplitude correlations, they we have not investigated in this paper (see [35] for a review of how common reference, volume conduction, field spread, or common input affect the quantification of the coordinated activity between brain regions). However, our analysis illustrates an approach for examining the effects of such phenomena on λ_2 (and hence on spectral structure) on multilayer functional networks, and we expect that one will observe similar qualitative phenomena in both multiplex and full multilayer networks constructed using other choices (e.g., difference measures than MI) from the ones that we chose to give a concrete illustration.

We initially studied the alpha-beta 2-layer network, because the alpha and beta bands are known to incorporate a large amount of the power spectrum of brain activity during resting state and they are the frequency bands that typically exhibit stronger synchronization between brain regions (e.g., see [21]). These bands are thus the most commonly-studied bands in resting-state studies, and we followed this tradition. Nevertheless, in our particular case, our comparison between 2-layer and 4-layer networks illustrates that the gamma band is the one that most influences the spectral properties of the full 4-layer multilayer network (see Fig. 8). As we showed in Table II, the theta and gamma layers, despite having weaker intralayer connectivities, are the ones with the largest percentage of interlayer connections (see the table caption), thus leading to the strongest correlation between a 2-layer network (with theta and gamma layers) and the complete (4-layer) multilayer network. This fact highlights the importance of the well-known phase-amplitude correlations between the theta and gamma frequency bands [30, 40], as the former acts as a carrier of fast amplitude fluctuations in the latter. Consequently,

theta-gamma coupling may be fundamental for understanding the multilayer nature of functional brain networks.

Finally, it is worth mentioning that although our results are concerned with resting-state MEG recordings, we expect to observe similar behavior in frequency-based multilayer networks of different origins — whether obtained from any of a large variety of different cognitive or motor tasks, with different brain-imaging techniques, or even if they come from a completely different system (such as functional climate networks [36]).

MATERIALS AND METHODS

Data Acquisition. Data sets have been made available by the Human Connectome Project (HCP); see [37] and [38] for details. The experimental data sets consist of the magnetoencephalographic (MEG) recordings of a group of 89 individuals, during resting state, for a period of approximately 2 minutes. During the scan, subjects were supine and maintained fixation on a projected red crosshair on a dark background. Brain activity was scanned on a whole head MAGNES 3600 (4D Neuroimaging, San Diego, CA, USA) system housed in a magnetically shielded room, and it included up to 248 magnetometer channels. The root-mean-squared (RMS) noise of the magnetometers is about 5 fT/sqrt (Hz) on average in the white-noise range (above 2 Hz). Data was recorded at sampling rate of $f_s \approx 508.63$ Hz. Five current coils attached to the subject, in combination with structural-imaging data and head-surface tracings, were used to localize the brain in geometric relation to the magnetometers and to monitor and partially correct for head movement during the MEG acquisition. Artifacts, bad channels, and bad segments were identified and removed from the MEG recordings, which were processed with a pipeline based on independent component analysis (ICA) to identify and clean environmental and subject’s artifacts [38].

Coordination between brain regions. To encode the coordination between brain regions, we first apply a band-pass filter to the preprocessed signals to obtain, for each of the N sensors, a set of four different time series, each of which corresponds to a specific frequency band: theta [3–8] Hz, alpha [8–12] Hz, beta [12–30] Hz, and gamma [30–100] Hz. We thereby obtain $4 \times N$ time series of 149646 points for each of the 89 individuals. We then order the filtered signals according to their corresponding frequency band, so $X^{(i \in \{1, \dots, N\})}$ corresponds to the theta band, $X^{(i \in \{N+1, \dots, 2N\})}$ corresponds to the alpha band, $X^{(i \in \{2N+1, \dots, 3N\})}$ corresponds to the beta band, and $X^{(i \in \{3N+1, \dots, 4N\})}$ corresponds to the gamma band. We calculate the mutual information (MI) between each pair of channels, X^j and X^k , with the for-

mula

$$\text{MI}_{X^j X^k} = \sum p_{lm} \log \left(\frac{p_{lm}}{p_l p_m} \right),$$

where p_{lm} is the joint probability distribution of finding $X^j = x_l$ and $X^k = x_m$ at the same time step. When X^j and X^k are independent variables, $p_{lm} = p_l p_m$, and the resulting MI is 0. However, when $X^j = X^k$ for all the series, MI achieves its maximum value. Note that $\text{MI}_{X^j X^k} = \text{MI}_{X^k X^j}$, so we obtain an undirected edge between the two time series and we are disregarding causality. Calculating MI allows one to detect coordinated activity even for time series that include different frequency bands. See [35, 39] for a review of different measures for quantifying coordination between brain regions and a discussion of their advantages and pitfalls. It is worth mentioning that $\text{MI}_{X^j X^{(j+N)}}$ is measuring the interplay between two different frequency bands in the same brain region j . Finally, MI is normalized with surrogates that we obtain with a block-permutation procedure [40]: each time series is simultaneously cut into blocks of 1018 points, and the resulting blocks are permuted uniformly randomly before again evaluating the MI between each time series. This yields MI_{rand} .

Frequency-based multilayer networks. We construct the frequency-based multilayer network for each individual from the matrix that contains the MI of each pair of sensors for the four different frequencies bands. Each layer includes nodes with the same frequency band, yielding four different layers: theta (θ), alpha (α), beta (β), and gamma (γ). Specifically, we construct a weighted supra-adjacency matrix \mathbf{W} whose elements are $W(i, j) = \text{MI}(i, j) - \text{MI}_{\text{rand}}(i, j)$ if $\text{MI}(i, j) > \text{MI}_{\text{rand}}(i, j)$ and 0 otherwise. In this way, we account only for edges with statistically significant edges. (In Fig. 2, one can see what fractions of edges are 0 in each case.) Finally, we apply a linear normalization to \mathbf{W} to obtain

$$\mathbf{M}(i, j) = \frac{w_{ij} - w_{\min}}{w_{\max} - w_{\min}},$$

where w_{\min} and w_{\max} are, respectively, the largest and smallest values of \mathbf{W} . This ensures that $\mathbf{M}(i, j) \in [0, 1]$ for each individual, which facilitating comparisons between them. The weighted supra-adjacency matrix \mathbf{M} contains some number of 0 entries, which account for interactions between brain regions and frequencies that we deem to not be statistically significant. It also has four blocks along the diagonal that encode interactions within each layer (i.e., the same frequency band at different brain regions), and it has off-diagonal blocks quantify coordination between different frequencies. See Fig. 1(b) for a schematic.

ACKNOWLEDGEMENTS

J.M.B. thanks John Allen for fruitful conversations. J.M.B. acknowledges financial support from Spanish

MINECO (project FIS2013-41057) and from Salvador de Madariaga Program (PRX15/00107), which allowed him

to visit University of Oxford in summer 2016.

-
- [1] Kivela, M., Arenas, A., Barthelemy, M., Gleeson, J. P., Moreno, Y. & Porter, M. A. Multilayer networks. *J. Cplx. Netw.* **2**, 203–271 (2014).
- [2] Boccaletti, S., Bianconi, G., Criado, R., Del Genio, C. I., Gómez-Gardenes, J., Romance, M., Sendina-Nadal, I., Wang, Z. & Zanin, M. The structure and dynamics of multilayer networks. *Phys. Rep.* **544**, 1–122 (2014).
- [3] De Domenico, M., Solé-Ribalta, A., Cozzo, E., Kivela, M., Moreno, Y., Porter, M. A., Gómez, S. & Arenas, A. Mathematical formulation of multilayer networks. *Phys. Rev. X* **3**, 041022 (2013).
- [4] Radichi, F. & Arenas, A. Abrupt transition in the structural formation of interconnected networks. *Nat. Phys.* **9**, 717–720 (2013).
- [5] De Domenico, M., Granell, C., Porter, M. A., & Arenas, A. The physics of spreading processes in multilayer networks. *Nature Phys.* **12**, 901–906 (2016).
- [6] Salehi, M., Sharma, R., Marzolla, M., Magnani, M., Siyari, P., & Montesi, D. Spreading processes in multilayer networks. *IEEE Trans. Netw. Sci. Eng.* **2**(2), 65–83 (2015)
- [7] Gómez, S., Díaz-Guilera, A., Gómez-Gardeñes, J., Pérez-Vicente, C. J., Moreno, Y. & Arenas, A. Diffusion Dynamics on Multiplex Networks. *Phys. Rev. Lett.* **110**, 028701 (2013).
- [8] Buldyrev, S. V., Parshani, R., Paul, G., Stanley, H. E., & Havlin, S. Catastrophic cascade of failures in interdependent networks. *Nature* **464**, 1025–1028 (2010).
- [9] Gao, J., Buldyrev, S. V., Stanley, H. E., Xu, X. & Havlin, S. Percolation of a general network of networks. *Phys. Rev. E* **88**, 062816 (2013).
- [10] Aguirre, J., Sevilla-Escoboza, R., Gutiérrez, R., Papo, D. & Buldú, J. M. Synchronization of interconnected networks: The role of connector nodes. *Phys. Rev. Lett.* **112**, 248701 (2014).
- [11] De Domenico, M. Multilayer modeling and analysis of human brain networks. *Gigascience*, doi:10.1093/gigascience/gix004 (2017).
- [12] Bassett, D. S. and Sporns, O. Network neuroscience. *Nature Neurosci.*, **20**, 20, 353–364 (2017).
- [13] Honey, C.J., Koötter, R., Breakspear, M., & Sporns, O. Network structure of cerebral cortex shapes functional connectivity on multiple time scales. *Proc. Natl. Acad. Sci. USA* **104**, 10240–10245 (2007).
- [14] Stam, C. J., van Straaten, E. C. W. , Van Dellen, E., Tewarie, P., Gong, G. , Hillebrand, A., Meier, J. & Van Mieghem, P. The relation between structural and functional connectivity patterns in complex brain networks, *International Journal of Psychophysiology* **103**, 149–160 (2016).
- [15] Battiston, F., Nicosia, V., Chavez, M., & Latora, V. Multilayer motif analysis of brain networks, <https://arxiv.org/abs/1606.09115> (2016).
- [16] Milo, R., Shen-Orr, S., Itzkovitz, S., Kashtan, N., Chklovskii, D. & Alon, U., Network motifs: Simple building blocks of complex networks, *Science* **298**, 824–827.
- [17] Simas, T., Chavez, M., Rodriguez, P. R. & Díaz-Guilera A. An algebraic topological method for multimodal brain networks comparisons. *Front. Psychol.* **6**, 904 (2015).
- [18] Bassett, D. S., Wymbs, N. F., Porter, M. A., Mucha, P. J., Carlson, J. M. & Grafton, S. T. Dynamic Reconfiguration of Human Brain Networks During Learning. *Proc. Nat. Acad. Sci. USA* **118**(18), 7641–7646 (2011).
- [19] Braun, U., Schäfer, A., Walter, H., Erk, S., Romanczuk-Seiferth, N., Haddad, L., Schweiger, J. I., Grimm, O., Heinz, A., Tost, H., Meyer-Lindenberg, A. & Bassett, D. S. Dynamic reconfiguration of frontal brain networks during executive cognition in humans. *Proc. Natl. Acad. Sci. USA* **112**, 11678–11683 (2014).
- [20] Buzsáki, G., Rhythms of the Brain, *Oxford University Press* (2006).
- [21] Brookes, M. J., Tewarie, P. K., Hunt, B. A., Robson, S. E., Gascoyne, L. E., Liddle, E. B., Liddle, P. F. & Morris, P. G. A multi-layer network approach to MEG connectivity analysis. *NeuroImage* **132**, 425–438 (2016).
- [22] De Domenico, M., Sasai, S. & Arenas, A. Mapping multiplex hubs in human functional brain network. *Front. Neurosci.* **10**, 326 (2016).
- [23] Van Mieghem, P. *Graph Spectra for Complex Networks*. Cambridge University Press (2011).
- [24] Newman, M. E. J. *Networks: An introduction*. Oxford University Press (2010).
- [25] de Pasquale, F., Della Penna, S., Snyder, A. Z., Lewis, C., Mantini, D., Marzetti, L., Belardinelli, P., Ciancetta, L., Pizzella, V., Romani, G. L., & Corbetta, M. Temporal dynamics of spontaneous MEG activity in brain networks. *Proc. Natl. Acad. Sci. USA* **107**, 6040–6045 (2010).
- [26] van Diessen, E., Numan, T., van Dellen, E., van der Kooij, A. W., Boersma, M., Hofman, D., van Lutterveld, R., van Dijk, B. W., van Straaten, E. C. W., Hillebrand, A. & Stam, C. J. Opportunities and methodological challenges in EEG and MEG resting state functional brain network research. *Clinical Neurophysiology* **126**, 1468–1481 (2015).
- [27] Fortunato, S. & Hric, D. Community detection in networks: A user guide. *Phys. Rep.* **659**, 1–44 (2016).
- [28] Almendral, J. A. & Díaz-Guilera, A. Dynamical and spectral properties of complex networks, *New J. Phys.* **9**, 187 (2007).
- [29] MacKay, D. *Information Theory, Inference, and Learning Algorithms*. Cambridge University Press (2003).
- [30] Aru, J., Aru, J., Priesemann, V., Wibral, M., Lana, L., Pipa, G., Singer, W. & Vicente R. Untangling cross-frequency coupling in neuroscience. *Curr. Opin. Neurobiol.* **31**, 51–61 (2016).
- [31] Erdős, P. & Rényi, A. On Random Graphs I. *Publications Mathematicae* **6**, 290–297 (1959).
- [32] Sahneh, F. D., Caterina Scoglio, C. & Van Mieghem, P. Exact coupling threshold for structural transition reveals diversified behaviors in interconnected networks. *Phys. Rev. E* **92**, 040801 (2015).
- [33] Barabási, A.-L. & R. Albert. Emergence of scaling in random networks. *Science* **286**, 509–512 (1999).

- [34] Kopell, N. J., Gritton, H. J., Whittington, M. A. & Kramer, M. A. Beyond the connectome: The dynamome. *Neuron* **83**(6), 1319–1328 (2014).
- [35] Bastos, A. M. & Schoffelen, J. M. A tutorial review of functional connectivity analysis methods and their interpretational pitfalls. *Front. Syst. Neurosci.* **9**, 175 (2016).
- [36] Tsonis, A. A., & Roebber, P. J. The architecture of the climate network. *Physica A* **333**, 497–504 (2004).
- [37] <https://www.humanconnectome.org>
- [38] Larson-Prior, L. J., Oostenveld, R., Della Penna, S., Michalareas, G., Prior, F., Babajani-Feremi, Schoffelen, J.-M., Marzetti, L., de Pasquale, F., Di Pompeo, F., Stout, J., Woolrich, M., Luo, Q., Bucholz, R., Fries, P., Pizzella, V., Romani, G. L., Corbetta, M. & Snyder A. Z. Adding dynamics to the Human Connectome Project with MEG. *NeuroImage* **80**, 190–201 (2013).
- [39] Pereda, E., Quiroga, R. Q. & Bhattacharya, J. Nonlinear multivariate analysis of neurophysiological signals. *Progress in Neurobiology* **77**, 1–37 (2005).
- [40] Canolty, R. T., Edwards, E., Dalal, S. S., Soltani, M., Nagarajan, S. S., Kirsch, H. E., Berger, M. S., Barbaro, N. M., & Knight, R. T. High gamma power is phase-locked to theta oscillations in human neocortex. *Science* **313**, 1626–1628 (2006).
- [41] In general, networks constructed from pairwise time-series similarities lead to nonzero edge weights in all (or almost all) intralayer adjacency entries [12]. However, in functional brain networks, the deletion of entries that are not statistically significant can lead to a non-negligible number missing edges, as is the case with our data sets.